Thickness noise of a propeller and its relation to blade sweep

By R. K. AMIET

10118 Dover Road, Apple Creek, OH 44606, USA

Linearized acoustic theory is applied to the calculation of the thickness noise produced by a supersonic propeller with sharp leading and trailing edges. The theoretical development is summarized and numerical calculations of the pressure–time waveform are presented. The erratic behaviour of previous time-domain calculations has been completely eliminated by careful numerical treatment of singular points, multiple singular points and nearly singular points that appear in the analysis. This allows a close inspection of the details of the calculated waveform and leads to the discovery of abrupt changes of slope in the pressure–time waveform, produced by singular points entering or leaving the blade at the tip. The behaviour of the pressure–time waveform is shown to be closely related to changes in the retarded rotor shape. Logarithmic singularities in the waveform are shown to be produced by regions on the blade edges that move towards the observer at sonic speed while at the same time having the edge normal to the line joining the source point and the observer. The logarithmic singularities are closely related to the shock waves produced by a swept airfoil in supersonic rectilinear motion, and they can be eliminated throughout the entire flow field by sweeping the rotor so that the Mach-number component normal to the leading and trailing edges is subsonic for all points on the rotor edges.

1. Introduction

The production of sound by a propeller due to the blade thickness is problem of current interest. A propeller achieves improved efficiency relative to typical turbofan aeroengines since a significantly greater rotor diameter is practical, but the production of noise is a significant drawback. This problem has received much attention in the literature, including the papers of Hawkings & Lowson (1974), Lowson & Jupe (1974), Farassat & Succi (1980), Farassat (1983, 1984, 1986), Hanson (1976, 1980), Schmitz & Yu (1986) and others. Much of the notation here follows that of Hanson (1976). These previous papers did not examine the detailed shape of the pressure–time waveform and its relation to the retarded blade shape. The accurate calculation of the pressure field has presented difficulties. Singular points and points that are nearly singular, if improperly treated, lead to erratic results in the calculations. Although the previous calculations may be satisfactory for acoustic predictions, the accuracy of the present prediction gives a better understanding of the sound production process.

The mathematical formulation of the problem is quite straightforward, although this may be obscured somewhat in the literature by several reformulations that attempt to avoid computational difficulties. The present analysis begins with the simplest formulation, accepting the computational difficulties, and uses appropriate

numerical techniques to properly treat the difficult areas. Thus, rather than reformulate the problem to avoid integrable singular points, the singular integrals are evaluated in a straightforward manner using techniques appropriate to the type of singularity.

The present calculation considers only the case of blade thickness. The loading or dipole case is not considered, but is quite easily included by replacing the expression for a monopole by that for a dipole in the analysis, assuming the dipole strengths are given. Because the retarded blade shape, which is critical in determining the radiated pressure field, does not depend on the source type, the dipole sound due to steady loading is not expected to introduce new effects. Axial mean flow is assumed and the blade thickness is simulated by monopoles placed on the helix, rather than on the actual blade surface, following standard linearized theory. Sharp leading and trailing edges are assumed. It should be possible to treat the blunt-edge case following a similar analysis; this case is expected to show the same close relation to the rectilinear motion case as does the sharp-edge case. The major factors have been retained, resulting in an improved understanding of the sound generation and several characteristics unique to this problem.

Some researchers may prefer a frequency-domain analysis, rather than the time-domain analysis presented here. Thus, Hanson's more recent treatment (1979) is in the frequency domain rather than the time domain used previously (1976). There are arguments for each approach. The frequency-domain approach avoids some of the numerical complexity of the time domain. However, if the results of the frequency domain are inverted back to the time domain, the singular peaks and abrupt slope changes in the pressure–time waveform require many frequency terms to get comparable resolution. An understanding of the origin of these singularities provides a promising avenue for noise attenuation. Although Tam (1983) analyses the case of an airfoil with a blunt leading edge in the frequency domain and is able to derive the singular behaviour for this case, the present author feels that a time-domain analysis gives a more physical understanding of these singularities and their point of origin on the blade. It will be seen that for any given observer position the singularities originate from a small region of the blade edge. Because a Fourier decomposition of the blade source term is made in the frequency-domain analysis, it becomes difficult to determine detailed source locations. Moreover, it seems more natural to regard the problem in the time domain since the waveforms from successive rotor passes are essentially independent non-overlapping pulses. Analysing the problem as a series of harmonics based on blade passage frequency may be relevant to the listener, but the introduction of the additional variable, blade passage frequency, has no direct relation to the properties of an individual pulse.

The formal solution to the problem is presented in §2. The behaviour of the resulting integral (which must be evaluated numerically) near certain singular points that arise is analysed in §3. The relation to a previous result of Taylor, Lamb and Hilton is given in §4. A brief description of the calculation procedure is given in §5 and the calculated results are analysed in §6. The case of zero sweep is first presented followed by cases with sweep, first a small amount then a more significant amount. Sweep is useful for eliminating logarithmic singularities in the pressure–time waveform caused by rotor edges having a supersonic relative velocity normal to the edge. Another type of behaviour characteristic of this problem is the occurrence of sudden changes of slope in the pressure–time waveform; the origin of these is explained in the analysis.

The present paper deals only with theory and does not make comparison with

experimental measurements. The object is to present a rigorous analytical and numerical result, showing the detailed behaviour of the exact linearized solution. This is shown to agree with a previous calculation of Hanson that gave the general form of the solution, but not the fine detail. For comparison of the linearized solution with experiment, the author is referred to the papers of Hanson (1979) or Schmitz & Yu (1986). These references show limitations of the linearized solution, especially where transonic effects become important. By clarifying and more rigorously investigating the linearized solution, it is hoped that the present paper will help form the basis for future investigations into these nonlinear effects.

2. Analytical formulation and solution

The simplest case of a propeller moving along a helical path without crossflow is analysed. The helix is formed by straight line generators; i.e. the intersection of the helix with the plane $x = $ constant is a straight line. The rotor blade is assumed to lie close to this helix; the sources used to represent the blade can then be assumed to lie in the helix, a standard linearized-flow assumption. The rotor hub moves along the x-axis as shown in figure 1. The leading edge of the rotor can be any curve, although initially it will be assumed to be a straight line coinciding with the y-axis at time $t = 0$. The chord c of the rotor can be a function of radius but is here assumed constant, and the blade thickness is denoted by $h(\cdot)$ with $h(0)$ denoting the leading edge and $h(c)$ the trailing edge. The thickness also can be a function of radius, but is set to zero at the leading and trailing edges; i.e. the edges are sharp. For any given radius r_0 the parameter γ is used to measure the distance along the helix. The γ-coordinate is fixed with the helix. It is set to zero on the y axis, and is positive in the downstream direction of the helix. Thus, $\gamma = 0$ coincides with the airfoil leading edge only at $t = 0$, as shown in figure 2. The observer is assumed to be fixed to the ambient fluid, the propeller moving past him. The helical surface along which the blade moves is then fixed with respect to the observer. The observer is taken to lie in the $z = 0$ plane; this loses no generality since the observer's x-position and time can be appropriately adjusted to give a situation equivalent to an arbitrary z-position.

The far-field pressure is written using the linearized form of the result of Curle (1955),

$$4\pi p = \frac{\partial}{\partial t}\int_S \rho_0 v_{\mathrm{n}}\left(\mathbf{y}, t - \frac{r}{c_0}\right)\frac{\mathrm{d}S}{r} - \frac{\partial}{\partial x_i}\int_S n_i p_{ij}\left(\mathbf{y}, t - \frac{r}{c_0}\right)\frac{\mathrm{d}S}{r}, \tag{1}$$

where S represents the surface that generates the sound, p_{ij} is the surface stress, v_{n} is the normal surface velocity, c_0 is the sound speed, n_i is the surface normal, ρ_0 is the free-stream density and r is the distance from source to observer. The airfoil is assumed to have no loading so that the force term is zero, leaving only the first term in (1). The second term could be included, if p_{ij} were known, but the integration would be over the same retarded surfaces as for the first term, giving much the same basic behaviour. Since the source term in the above equation has an arbitrary time dependence, a moving body can be represented by stationary sources turning on and off to represent the flow field generated by a body moving past.

Relative to the blade, the fluid velocity normal to the surface is equal to the local fluid velocity relative to the body surface times the body slope along the direction of the velocity. Because the perturbations are assumed small, the fluid velocity along the helical surface relative to the rotor is set equal to the negative of local rotor velocity; that is, relative to the helix the local fluid does not move in the airfoil plane
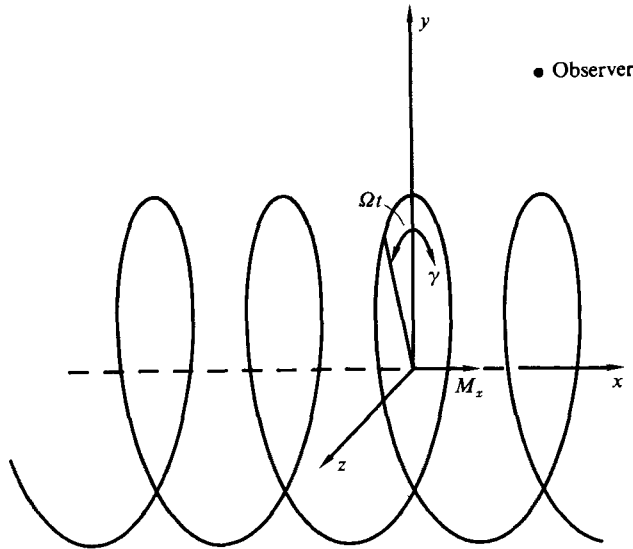
FIGURE 1. Helical path of path of propeller in the fluid-fixed coordinate system showing the origin of the γ-variable relative to the blade leading-edge position at time $t = 0$.
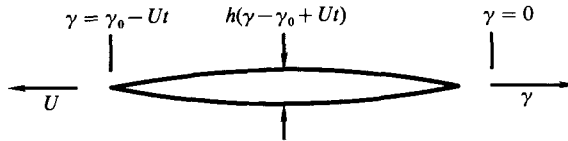

FIGURE 2. Thickness distribution of the blade (shown to scale) used for all calculations in this paper. Position of the blade leading edge relative to the γ-axis is shown.

to lowest order. Using the coordinate γ the airfoil thickness for a given radial station is $h(\gamma - \gamma_0 + Ut, r_0)$. Equation (1) for the pressure can then be written

$$
4\pi p = \rho_0 U \frac{\partial}{\partial t} \int_0^s \int_{-\infty}^{\infty} \frac{h'(f, r_0)}{R} \, d\gamma \, dr_0
$$

$$
= \rho_0 U^2 \int_0^s \int_{-\infty}^{\infty} \frac{h''(f, r_0)}{R} \, d\gamma \, dr_0, \tag{2}
$$

where
$$
f \equiv \gamma - \gamma_0(r_0) + Ut - M_r R, \quad M_r \equiv \frac{U}{c_0}, \quad h'' \equiv \frac{\partial^2 h}{\partial \gamma^2}, \tag{3}
$$

r_0 is the radial position on the rotor, s is the rotor span, U is the velocity of the blade segment relative to the fluid and $\gamma_0(r_0)$ is the γ-distance of the airfoil leading edge from the y-axis at $t = 0$; for a straight blade $\gamma_0 = 0$. In effect, γ_0 is a phasing term to account for sweep; the sound for any given dr_0 blade segment can be calculated by assuming $\gamma = 0$ at $t = 0$ and then time shifting to the actual γ-value using γ_0. The distance R of the observer to a point r_0, γ on the helix is

$$
R^2 = \left(x + \frac{\gamma V}{U}\right)^2 + y^2 + r_0^2 - 2yr_0 \cos\left(\frac{\gamma \Omega}{U}\right). \tag{4}
$$

The velocity V represents the forward flight speed along the x-axis. For a rotor with

a radian velocity Ω, the azimuthal velocity at a radius r_0 is Ωr_0 and $U^2 = V^2 + \Omega^2 r_0^2$. The γ-integration in (3) is taken over the entire γ-range, $-\infty < \gamma < \infty$. For any given time the γ-values satisfying $f = 0$ and $f = c$ represent retarded positions of the airfoil leading edge and trailing edge respectively. (The curves of $r_0 = $ constant and $\gamma = $ constant are not orthogonal since $\gamma = $ constant does not represent a line of constant azimuthal angle θ. Nevertheless, the figure enclosed by the lines $r_0, r_0 + \mathrm{d}r_0, \gamma$, and $\gamma + \mathrm{d}\gamma$ is a parallelogram, the height given by $\mathrm{d}r_0$ and the base by $\mathrm{d}\gamma$; the differential area is $\mathrm{d}r_0 \,\mathrm{d}\gamma$, as required in (2).) The first form of (2) for the pressure was used by Hanson (1976), and much of the notation here follows that paper, but the present calculation is based on the second form.

The second relation in (2) results from taking the time derivative under the integrals where it operates on Ut in the argument f. Although both forms should give identical answers, the second form is used since the integrals are rather sensitive to errors, and it should be preferable to use a form that does not need to have the time derivative taken after numerical evaluation of the integral. However, the integrand of the second form becomes infinite at the airfoil leading and trailing edges since h'' is infinite here; h' is finite since the airfoil is assumed to have sharp leading and trailing edges. This would make the second form of (2) more difficult to evaluate, except for the fact that the difficult points are much more evident and can be properly accounted for, whereas in the first form the integral may appear easier, but difficulties arise on taking the derivative.

The infinity of h'' at the leading and trailing edges is eliminated by performing the γ-integral after introducing the delta function form

$$h''(\gamma, r_0) = h'(0, r_0)\,\delta(\gamma) + h_1''(\gamma, r_0) - h'(c, r_0)\,\delta(\gamma - c). \tag{5}$$

The derivatives of the thickness, $h'(0, r_0)$ and $h'(c, r_0)$, represent the total angle between tangents to the upper and lower surfaces at the airfoil edges. h' at the leading edge is positive and h' at the trailing edge is negative. h_1'' is assumed to be zero ahead of the leading edge and behind the trailing edge, and there is at most a finite discontinuity in h_1'' at the edges. Equation (5) gives the correct result for h' and h if integrals of h'' over γ are performed.

With the substitution of (5), equation (2) becomes

$$p(x, t) = \frac{\rho_0 U^2}{4\pi} \int_0^s \left[\int_{-\infty}^{\infty} h''(f, r_0) \frac{\mathrm{d}\gamma}{R} + \frac{h'(0, r_0)}{\left(R \left| 1 - M_r \dfrac{\partial R}{\partial \gamma} \right| \right)_{f=0}} - \frac{h'(c, r_0)}{\left(R \left| 1 - M_r \dfrac{\partial R}{\partial \gamma} \right| \right)_{f=c}} \right] \mathrm{d}r_0. \tag{6}$$

The integrand of the double integral is always finite. The integrands of the single integrals become infinite when the denominators become zero; i.e. when

$$\frac{\partial f}{\partial \gamma} = 1 - M_r \frac{\partial R}{\partial \gamma} = 0 \tag{7}$$

with the constraint $$f = \langle c \rangle, \tag{8}$$

where the notation $\langle c \rangle$ is defined to be 0 for the leading edge and c for the trailing edge. The solution of (8) is the γ-value for the given t and r_0 that lies on the leading or trailing edges. The locus of all such points for r_0-values between the hub and the tip $(0 < r_0 < s)$ is the retarded blade shape, shown in figures 6, 11 and 13. Points on the blade edge satisfying (7) are moving towards the fluid-fixed observer at a relative Mach number of one. These might be expected to be very significant points, but in

the analysis to follow it is shown that this depends greatly on the blade sweep at the points.

3. Behaviour of the integrand near a singular point

3.1. Case of an integrable singular point

The last two terms in the integrand of (2) become infinite at singular points given by (7). This could create convergence problems for the r_0-integration if the behaviour near a singular point were of a power equal to or stronger than r_0^{-1}. It is shown below that the behaviour near a singular point is $r_0^{-\frac{1}{2}}$ with one exception as noted.

Consider the second term in the integrand of (7). (The third term is treated in the same manner.) Since this term is subject to the condition $f = 0$, it follows that between any two points on the leading edge

$$\Delta f = 0 = \Delta(\gamma - \gamma_0) - M_r \Delta R + (c_0 t - R) \Delta M_r. \tag{9}$$

In this equation the variation ΔR for variations $\Delta\gamma$ and Δr_0 is written using a Taylor's series as

$$\Delta R = \frac{\partial R}{\partial \gamma} \Delta\gamma + \frac{1}{2} \frac{\partial^2 R}{\partial \gamma^2} (\Delta\gamma)^2 + \frac{\partial R}{\partial r_0} \Delta r_0 + \dots . \tag{10}$$

The derivatives in (10) are to be evaluated at the singular point given by (7). Substitution of (10) into (9) and using (3) with $f = 0$ gives for the behaviour on the leading-edge edge near the singularity

$$\frac{\partial^2 R}{\partial \gamma^2} (\Delta\gamma)^2 + \frac{2}{M_r} \left[M_r \frac{\partial R}{\partial r_0} + \frac{(\gamma - \gamma_0) M_\theta^2}{r_0 M_r^2} + \chi \right] \Delta r_0 + \dots = 0, \tag{11}$$

where $M_\theta \equiv \Omega r_0 / c_0$. Also, ΔM_r was evaluated in terms of Δr_0 and $\Delta\gamma$ using $M_r^2 = V^2/c_0^2 + M_\theta^2$; locally the sweep parameter γ_0 is assumed to vary linearly with r_0; i.e. $\Delta\gamma_0/\Delta r_0 = \chi$. Equation (11) shows that, for points on the edge, $\Delta\gamma$ and Δr_0 are related by

$$\Delta\gamma \sim (\Delta r_0)^{\frac{1}{2}} \tag{12}$$

near the singular point. The behaviour of the second or third terms of (6) near the singular point is now found by expanding the denominator in a Taylor's series and using (12). Since $R|\partial f/\partial\gamma| = 0$ at the singular point, this gives for the denominator

$$\frac{\partial}{\partial\gamma}\left(R \left| \frac{\partial f}{\partial\gamma} \right| \right) \Delta\gamma + \frac{\partial}{\partial r_0}\left(R \left| \frac{\partial f}{\partial\gamma} \right| \right) \Delta r_0 + \dots = C_1 (\Delta r_0)^{\frac{1}{2}} + C_2 \Delta r_0 + \dots, \tag{13}$$

where C_1 and C_2 are non-zero constants. Near the singular point this expansion of the denominator shows the dominant behaviour of the second or third term in the integrand of (6) to be $(\Delta r_0)^{-\frac{1}{2}}$. This was previously found by Amiet (1977) from numerical calculations near the singular points. Thus, (6) is integrable over r_0 at the singular points, except as noted below. Nevertheless, the position of the singular points must be determined when numerically evaluating the integral, since special precautions are required for integration near singularities. Farassat (1983) has also investigated the behaviour of the integrand near the singular points. The notation is different enough that no direct comparison with the present result is readily possible, but the statement is made that the line integrals are integrable, which agrees with the above result, but overlooks the special case noted below.

3.2. *Case of a non-integrable singular point*

This inverse square-root behaviour near a singular point no longer holds if the coefficient of Δr_0 in (11) becomes zero. The condition for this is

$$M_r \frac{\partial R}{\partial r_0} + \frac{(\gamma - \gamma_0) M_t^2}{r_0 M_r^2} + \chi = 0. \tag{14}$$

When this holds, $\Delta \gamma \sim \Delta r_0$ and the denominator in (13) varies linearly with r_0 to lowest order. This produces an r_0^{-1} behaviour of the integrand, leading to a logarithmic singular behaviour near certain points in the pressure–time waveform which is evident in the figures to be shown. This behaviour was previously mentioned by Hawkings & Lowson (1974) who deduced the behaviour from the fact that when the calculations are made in the frequency domain, the asymptotic behaviour of the nth harmonic at these points is n^{-1}. The logarithmic behaviour is also stated without proof by Farassat (1986).

An analytical expression for the far-field pressure near the logarithmic singularity could be derived from appropriate expansions at a time very near the logarithmic singularity, following the above line of analysis. The result appears to be somewhat involved, and would probably be of little use; the singularity is only logarithmic and one must be quite near the singularity in order for this logarithmic behaviour to dominate the first term in the integrand, which cannot generally be evaluated in closed form. The analysis was carried out far enough to demonstrate the logarithmic behaviour $\ln (t - t_0)$, where t_0 is the time of occurrence of the logarithmic singularity. Note that $[\ln (t - t_0)]^2$ is integrable in time, assuring a finite value for the acoustic energy at the logarithmic singularities.

It should be emphasized that the term 'singularity' is being used in two different ways. The first usage denotes a singularity in the integrand of (6). If this is integrable over r_0, the second type of singularity will not appear. Equation (13) gives the behaviour of the integrand as, generally, $r_0^{-\frac{1}{2}}$; however, at certain values of r_0 and t the behaviour of the integrand becomes r_0^{-1}, leading to a logarithmic singularity in the pressure–time waveform. To distinguish between these two uses of singularity, the second type will always be denoted by the term 'logarithmic singularity'.

Equation (14) can give physical insight into the sound generation process. However, the variable γ has no simple relation to the geometry of the rotor; the equation becomes much clearer if reformulated in terms of the independent variables r_0, τ rather than the variables r_0, γ, where

$$\gamma - \gamma_0 = -U\tau; \tag{15}$$

$\gamma = \gamma_0$ at $t = 0$ for points on the leading edge, by definition of γ_0. At later times, for points on the leading edge the value of $\gamma - \gamma_0$ depends on r_0 whereas τ is a function only of time. Thus, a partial derivative with $\tau = $ constant is a derivative taken along the edge. Transforming from r_0, γ to r_0, τ gives

$$\left. \frac{\partial R}{\partial r_0} \right|_\gamma = \left. \frac{\partial R}{\partial r_0} \right|_\tau + \left. \frac{\partial R}{\partial \tau} \right|_{r_0} \left. \frac{\partial \tau}{\partial r_0} \right|_\gamma. \tag{16}$$

Figure 3 illustrates the blade orientation relative to the observer at the time of a logarithmic singularity. It is shown as a plane figure ($M_x = x = 0$) for simplicity only; the analysis does not require this. Line AB denotes the tangent to the blade leading edge at point D. OA is the blade reference line that coincides with the y-axis
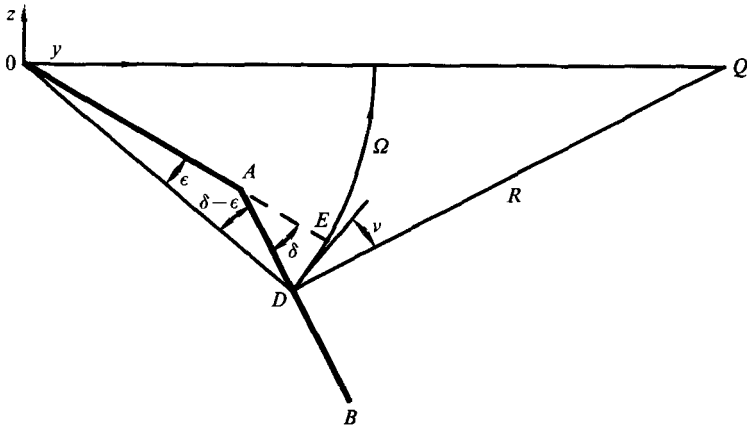
FIGURE 3. Position of the blade at the retarded time that produces a logarithmic singular point in the pressure–time waveform.

at $t = 0$. Lines $0A$ and AB need not be coincident with the rotor leading edge, except at point D, but for clarity it may be easier to think of the rotor leading edge as being composed of these two segments. The lines AB and QD are drawn normal to one another; this will be shown to be necessary if point D is a solution to (14). Taking the derivative of (15) with γ kept fixed and noting that $U^2 = V^2 + \Omega^2 r_0^2$ gives

$$\frac{\partial \tau}{\partial r_0}\bigg|_\gamma = -\frac{\tau}{r_0}\frac{M_t^2}{M_r^2} + \frac{\chi}{U}, \tag{17}$$

where $\chi = \partial \gamma_0/\partial r_0$. The derivative $\partial R/\partial \tau$ in (16) is found from (7); with the transformation in (15) this becomes

$$\frac{\partial R}{\partial \tau}\bigg|_{r_0} = -c_0. \tag{18}$$

Introducing (17) and (18) into (16) and using the result to replace the derivative in (14) cancels the second and third terms in that equation, leaving

$$\frac{\partial R}{\partial r_0}\bigg|_\tau = 0. \tag{19}$$

This is simply a restatement of (14) in a more suitable coordinate system. It shows that the change of R for small changes of position along the rotor edge is zero at location D where the logarithmic singularity is produced. That is, the line R from the observer at Q to the source point D is normal to the leading edge. If (7) alone is satisfied at some point D, there will be a singular point at D in the r_0-integral of (6). Equation (7) always has a solution (at some time) for points on the blade at a radius greater than the minimum sonic radius. This does not guarantee a singular point in the pressure–time waveform; only if (19) is also satisfied will a singular point be produced upon integration of (6). Thus, for a given observer position a logarithmic singularity is produced by some point D on the edge if the Mach number of the segment is sonic relative to the fluid-fixed observer and the blade edge at D is normal to the line from the observer to D.

3.3. *Discussion of the singularities*

The effect of sweep on the reduction of a propeller harmonic was previously attributed to phasing of the various spanwise segments (Hanson 1980). This is a satisfactory description, but the present analysis gives a more physical description in terms of the component of relative Mach number M_n normal to the edge. With a little thought it becomes evident that if $M_n > 1$ at any point D on the edge, then this point produces a logarithmic singularity at some point in the field. To see this, let the observer lie instantaneously in the plane normal to the edge at point D. In this plane the maximum Mach number of point D relative to the fluid fixed observer is M_n. If the observer moves in this plane towards the x-axis, the relative Mach number of point D decreases until it reaches the value 1; here the observer sees a logarithmic singularity since the edge is still normal to the line from the observer to D, satisfying (7) and (19). Thus, the faster moving outboard portion of the rotor tends to beam the sound up more towards the x-axis, just as the shock angle produced by an airfoil in rectilinear motion becomes smaller and the angle of propagation is in a more upward direction as the velocity increases. To eliminate logarithmic singularities from the entire flow field requires a subsonic edge, $M_n < 1$, for the entire rotor.

For illustration, consider the case $M_x = 0$, a rotor with no forward velocity, and determine the minimum blade sweep that avoids logarithmic singularities. An observer in the plane $x = 0$ places the strongest restriction on the blade shape since only in this plane will the Mach number in the direction of the observer reach its maximum. A line from the observer to any point on the rotor leading edge is normal to the leading edge at some time during the rotor rotation. Denoting the local blade sweep by $\nu(r_0)$ as in figure 3 (where ν is measured from the normal at D so that $\nu = \delta - \epsilon$), the Mach number in the direction of the observer at this time is $M_\theta \cos \nu$. The above discussion shows that there is no logarithmic singularity if and only if for all values of r_0

$$M_\theta \cos \nu < 1, \tag{20a}$$

where $M_\theta \equiv \Omega r_0/c_0$. The minimum sweep that still avoids a logarithmic singularity follows by taking the equality in (20a). The local sweep is related to infinitesimal changes dr_0 and $d\theta$ by

$$dr_0 = (r_0 \, d\theta) \cot \nu. \tag{20b}$$

Equation (20b) with an equality in (20a) gives for a blade shape with minimum sweep

$$\theta = (M_\theta^2 - 1)^{\frac{1}{2}} - \tan^{-1} (M_\theta^2 - 1)^{\frac{1}{2}}. \tag{20c}$$

Using linear analysis to calculate the pressure produced by this blade shape may give somewhat inaccurate results; every point on the edge of the blade is essentially transonic since the Mach-number component normal to the edge has the value one, and a transonic theory may be needed.

The above argument for the case $M_x = x = 0$ is easily generalized to the case $M_x \neq 0$. Considering a particular rotor radius r_0, if a plane is drawn normal to leading edge at this point an observer will find that in this plane the maximum value of the rotor Mach number M_n relative to the fluid-fixed observer is

$$M_n = [(M_\theta \cos \nu)^2 + M_x^2]^{\frac{1}{2}}, \tag{21}$$

where the sweep angle ν is defined as the angle between two planes, both normal to the $x = 0$ plane, with one tangent to the blade leading edge at the point r_0 and the second passing through the x-axis and the point r_0 on the leading edge; (20b) is

consistent with this definition. There will be no logarithmic singularity if $M_n < 1$, giving $(M_\theta/\beta) \cos \nu < 1$, where $\beta^2 \equiv 1 - M_x^2$. The rest of the derivation follows as before with the result that in $(20c)$ M_θ becomes M_θ/β.

Comparison with the two-dimensional case of a swept airfoil is very helpful. If an infinite-span airfoil moves rectilinearly at supersonic speed but is swept so that the velocity normal to the leading edge is subsonic, then, ignoring boundary-layer effects, one can translate parallel to the airfoil, eliminating the spanwise flow component and making the problem subsonic. One might calculate the sound from such an airfoil by integration over the span, just as is done here. For a fluid-fixed observer the integration produces 'singular points' where the relative Mach number of that spanwise segment is sonic relative to the observer. However, since the far-field pressure perturbation of an airfoil moving rectilinearly at subsonic speed is zero, these local singular points have no particular significance. There will be significant phasing differences between the various spanwise segments giving noise cancellation, whereas if the problem were calculated in a coordinate system in which the airfoil moved normal to its leading-edge line, there would be no need for this phasing interpretation.

This singular behaviour can be compared to a shock wave from the edge such as occurs for a two-dimensional airfoil in supersonic flow. This should be considered a qualitative analogy, however, since the pressure field calculated for linearized flow over a two-dimensional airfoil does not give an infinite pressure at the shock; rather only a jump in pressure is predicted. The logarithmic singularity of the rotor case is a focusing of the Mach-wave pressure field not present in the two-dimensional case. Nevertheless, the criterion for a logarithmic singularity for the rotor case is the same criterion for an observer to lie on the shock produced by an airfoil in rectilinear motion. That is, the observer lies on the shock at that time when the airfoil at the retarded position is moving towards the observer at a relative Mach number of one. Also, the requirement that $M_n < 1$ for all r_0 to eliminate logarithmic singularities throughout the fluid is the same criterion for a swept airfoil in rectilinear motion to produce no shock.

The predictions for the rotor problem near the logarithmic singularities must be regarded as inaccurate to some degree since an infinite pressure cannot actually exist. This is another reason for favouring the time-domain approach over the frequency-domain approach. Since the linearized solution must be in error near the logarithmic singularities, these points are easily excluded from comparisons with experiment when in the time domain. In the frequency domain, however, the errors made near the logarithmic singularities are mixed throughout the spectrum, and the only way to remove them is to perform a Fourier inversion to the time domain. This may not be especially important in practice since a rotor should be designed to avoid the logarithmic singular points; also the logarithmic singularities are integrable, giving only finite acoustic energy. Nonlinear propagation may also be easier to account for using the time-domain approach. The inaccuracy in the linearized solution for the prediction of the logarithmic singularities was noted by Hanson (1979) by comparison with data, although the singular behaviour at these points was not noted.

A singular point entering or leaving the rotor at the tip also produces a significant effect worth consideration. The singular points change their radial position on the blade during the rotation of the rotor. Since their velocity along the edge is affected by the blade velocity, sweep and observer position, but not the presence of the tip, their velocity at the tip is generaly non-zero, and one might expect a significant effect as a singularity moves past the tip. In fact, this phenomenon leads to abrupt changes

in the slope of the pressure–time waveform. The further description of this effect is delayed until §6.3, after the figures showing the movement of the singular point along the edge are presented.

4. Relation to the Taylor, Lamb, Hilton result

The pressure wave produced by the logarithmic singularity can be related to the wave discussed by Hilton (1938) who presents an analytical description (attributed to G. I. Taylor and H. Lamb) of the shape of the wave propagating at the sound speed away from the rotor and rotating with the angular velocity Ω of the rotor. Hilton considers the singular wave produced in the rotor plane by a single source point rotating supersonically in a circle with zero forward velocity. This produces two branches of the wave, one that moves outward from the source and one that moves inward towards the hub until reaching the sonic circle; here a cusp is produced and the wave again moves outward. A single source thus leads to two singular waves propagating to the far field.

For the cases considered here there are two source regions, one on the leading edge and one on the trailing edge. Each leads to only one singular wave, as is evident from the pressure–time waveforms at the observer, to be shown later; two logarithmic singularities are shown in figures 9 and 12, one arising from the leading edge and one from the trailing edge. For a straight blade, the source region is at the sonic circle (at the cusp described by Hilton); thus, the wave does not propagate inward from the source region and only a single wave is produced. For the swept-blade case, the region inboard of the source region is effectively moving subsonically owing to the sweep, and again only a single wave is produced. The present analysis shows that a single source is insufficient to define the wavefront; rather, it is necessary to know the distribution of sources in a region to understand the noise generation potential of that region. This is just a restatement of the fact that an airfoil moving at sonic speed towards the observer may or may not be an important noise source, depending on the sweep angle of the edge. This is acknowledged by Hilton, in effect, because of the obvious difficulty in determining which source, from all those on the airfoil surface, to use in determining the wavefronts that he measures. Hilton notes that the analysis of Taylor does not require the specification of a particular source, but that at the same time, the angular position at which to begin the wavefront is undetermined. This leads him to the comment 'It is better to regard these spiral curves as the only wave pattern which can rotate about the hub without change of shape, and to leave the relative positions of the airscrew blade and wave pattern to be determined by experiment'. The present paper gives the means to locate these spiral curves in relation to the rotor, at least to the accuracy permitted by the assumption of linearized flow.

It should be emphasized that the present derivation considers only the case of an airfoil with a sharp leading edge. Whereas Hilton places the source of the singular wave at the supersonically moving tip, for the present case the tip does not lead to such a singular wave; for a sharp leading edge the tip will later be shown to produce an infinite slope in the pressure–time plot at the time that the tip moves towards the observer at a Mach number of one (at the time a singular point moves past the tip), not a pressure jump or an infinite pressure. For the case of an airfoil with a finite leading-edge radius, however, the possibility of such a source at the tip cannot be excluded. In fact, the analysis of Tam (1983) suggests that pressure jumps may be produced by the tips of rotors with a finite leading-edge radius.
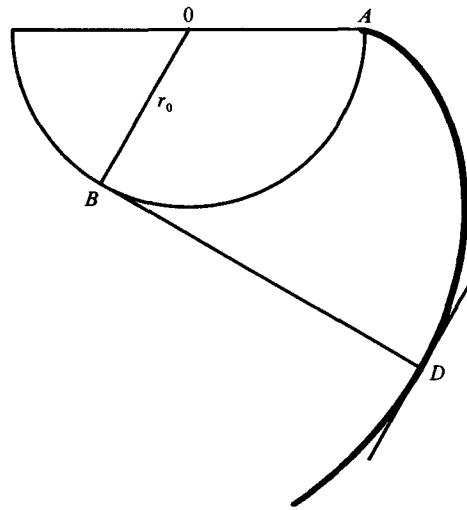
FIGURE 4. Path of the singular wave propagating away from the blade.

The construction procedure for the curve of the singular wavefront helps clarify its generation when one notes that the wavefront is produced at that time when the edge is normal to the source–observer line and moves at sonic speed towards the observer. The construction procedure given by Lowson & Jupe (1974), which involves drawing a series of circular arcs with centres on the moving source point, is consistent with this generation process. For the straight-blade case with $M_x = 0$ and the observer in the rotor plane, the present analysis shows that the source of the singular wave moves sonically. The curve in figure 4 is constructed by specifying the propagation distance of the wave, BD, to be equal to the length of arc AB through which the source has moved. Since the distribution of sources along the edge is normal to the source–observer line, the wavefront at its point of origin, B, is normal to this line. Because a wave propagates along its normal, this wave propagates to point D, defining the wavefront at D.

In figure 4 the wave at A is parallel to the leading edge, $0A$, of the straight blade. For the swept-blade case the wave is again parallel to the airfoil edge at the singular point on the blade, which is the origin of the wave. Just as for the straight-blade case this follows from the fact that the logarithmic singularity is produced by that point on the blade that moves towards the observer at sonic speed while having the edge normal to the source–observer line. The wave produced moves at sonic speed along a line normal to the wave. Since its direction of propagation must be towards the observer if it is to reach the observer, the wavefront is parallel to the edge at the point of generation.

5. The general method of calculation

A computer program for performing the integrations in (6) has been developed. This is a difficult programming task as is evident from the previously calculated results for this problem. For example, Farassat (1986) in his figure 3 compares results of a previous calculation with an improved calculation procedure. The improved procedure produces much better results, but the curves are still not perfectly smooth. Amiet (1977) points out the difficulties inherent in the time-domain calculation and

improves upon a previously calculated result of Hanson, but does not completely eliminate the errors. These errors can mask some of the behaviour to be discussed here, such as changes of slope that would be difficult to discover without an accurate prediction scheme. Without a reliable calculation, one is not certain whether the ragged prediction is due to numerical inaccuracies or inherent in the solution.

An alternative approach is to analyse the problem in the frequency domain. This should give identical results to the time-domain approach, after a Fourier inversion, if enough frequency terms are calculated. However, a great many terms would be required to illustrate the slope discontinuities shown in the following figures. Certain of the calculated points given here have a spacing of 0.01°; to get equivalent accuracy in the frequency domain would require of the order of 0.5 (360/0.01) harmonics. To some extent this accuracy is academic; i.e. it may not be needed for noise prediction. However, it is very useful when attempting to understand the sound generation process.

The computer program, consisting of approximately 600 lines of Fortran code, was developed and all calculations were performed on an Apple Macintosh Plus microcomputer. Calculations take on the order of twenty minutes per point for the pressure–time waveform on this computer, but this is highly dependent on the accuracy required, here specified as approximately fourth-digit; the calculation time could be significantly decreased by relaxing the accuracy requirement. Double precision arithmetic was used for all calculations; because of the many parts of the program where accuracy can be lost (finding zeros, integration of functions that tend to cancel to zero, etc.) this gives an extra margin of flexibility.

The program simulates a 'flyover' with the observer fixed to the ambient fluid; the result for a propeller-fixed observer can be calculated by translating the observer with the propeller and calculating the pressure for the corresponding stationary observer at each instant of time, since the motion of the observer does not affect the instantaneous pressure at the observer position.

The calculation begins with determination of the sonic line, given by (7), representing the locus of rotor points that are sonic with respect to the observer. The case of an observer fixed to the ambient fluid is simpler than the rotor-fixed-observer case since the helical path is fixed with respect to the fluid-fixed observer; this allows a single calculation (valid for all time) of the sonic line. A given point on the edge of the rotor is sonic with respect to the observer at the time when the point lies on this line.

For the case of zero forward velocity and an observer in the far field, the sonic line, $\partial f/\partial \gamma = 0$, is a straight line. To show this, set $V = 0$ in (4) and take the γ-derivative, giving $R(\partial f/\partial \gamma) = (\Omega y r_0/U) \sin(\gamma \Omega/U)$. If θ denotes the angular position around the rotor, then $\theta = \gamma \Omega/U$. Combining these two relations with (7), gives, for the equation of the sonic line,

$$r_0 \sin(\theta) = \text{constant}, \tag{22}$$

which is the equation of a straight line. The far-field assumption is needed to make small any relative changes in the factor R, contained in the constant on the right-hand side. The sonic-point locus is plotted as a dashed line in the figures of the retarded blade shapes, and is nearly a straight line since $V = 0$ is assumed for these results and the observer distance is significantly larger than the rotor radius.

To perform the r_0-integration in (6), the retarded position of the leading and trailing edges for the chosen observer position and time of interest must be found. This involves finding zeros of the function $f = \langle c \rangle$. Whereas the sonic line need only be calculated once for a fluid-fixed observer, the retarded blade shapes must be
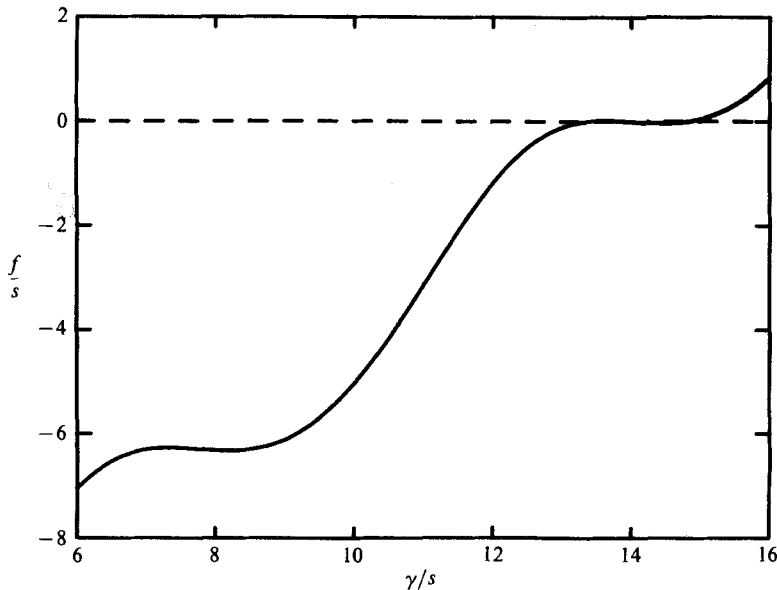
FIGURE 5. Plot of the function f versus θ showing three zeros at $\gamma/s = 13.33$, 14.00, 14.83. The parameters chosen for this particular calculation are $\Omega r_0/c_0 = 1.1$, $r_0/s = 1$, $y/s = 10$, $x = M_x = 0$, $(\Omega t/2\pi) \times 360 = -177.4$.

calculated for each new time point calculated. A sample plot of the function f, representing approximately two rotor rotations, is given in figure 5. The values listed for the parameters are the same values used later for the calculated sound; this is the case $V = 0$ for which f is a linear plus a cosine function of γ. Given the retarded blade position, the r_0-integral is calculated. This is conceptually simple, but it is the procedure most likely to give inaccuracies because of the singular points, points that are nearly singular and multiple singular points that are encountered in (6).

6. Calculated results

6.1. *The retarded blade shapes*

Plots of the retarded body shape (the retarded positions of each source point on the body for the time of interest) give insight into the sound production process. This type of plot was also given by Hanson (1976); it is a natural type of plot to make since locating the points satisfying $f = \langle c \rangle$ is a necessary intermediate step in evaluating (6). To make plotting easier, the forward velocity of the rotor is assumed zero so that the retarded body shape lies in a plane. This case was also chosen to match that of Hanson (1976), allowing a direct comparison of results.

Figure 6 shows a sequence of these retarded body shapes for the case of an airfoil with straight leading and trailing edges and a constant chord. The observer lies in the same plane as the counterclockwise turning rotor. Only the advancing half of the rotor disk is shown. The sonic line, plotted in these figures as a dashed line, points towards the observer; it would be exactly vertical if the observer were at infinity on the axis, but here the observer is only 5 rotor diameters away. The retarded airfoil shape is significantly distorted from the actual blade shape, and in fact can become divided into multiple regions. The successive figures are for increments of the rotation angle θ differing by $1°$ (equal time increments), except for figure $6(c)$ which
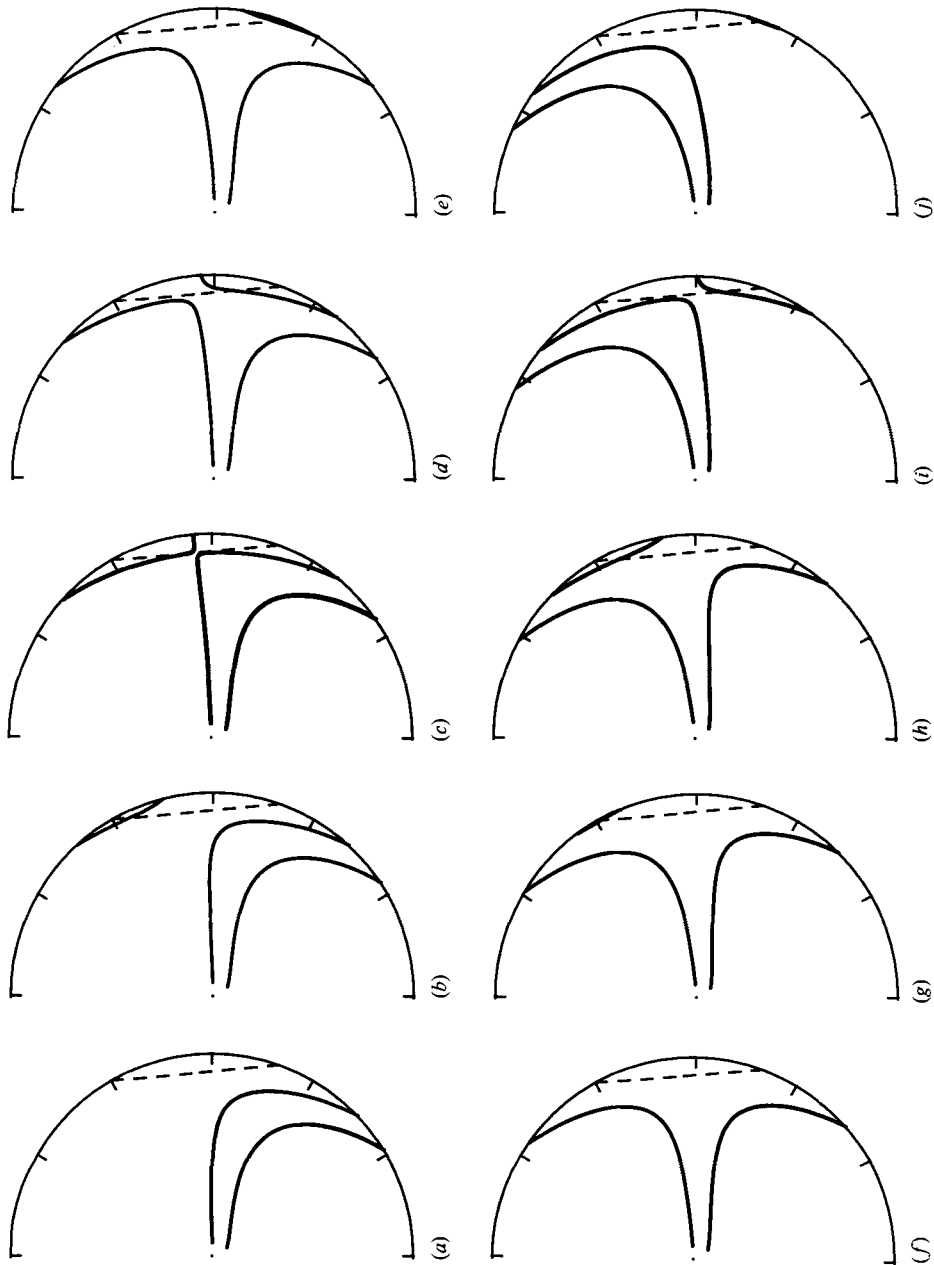
FIGURE 6. Retarded blade shapes for the straight-blade case. The parameters $\Omega r_0/c_0$, y/s, x, M_x take the same values as in figure 5; also $s/c = 12.5$. The sonic line is dashed. (*a*) $\theta = -179$; (*b*) -178; (*c*) -177.15; (*d*) -177; (*e*) -176; (*f*) -175; (*g*) -174; (*h*) -173; (*i*) -172; (*j*) -171.
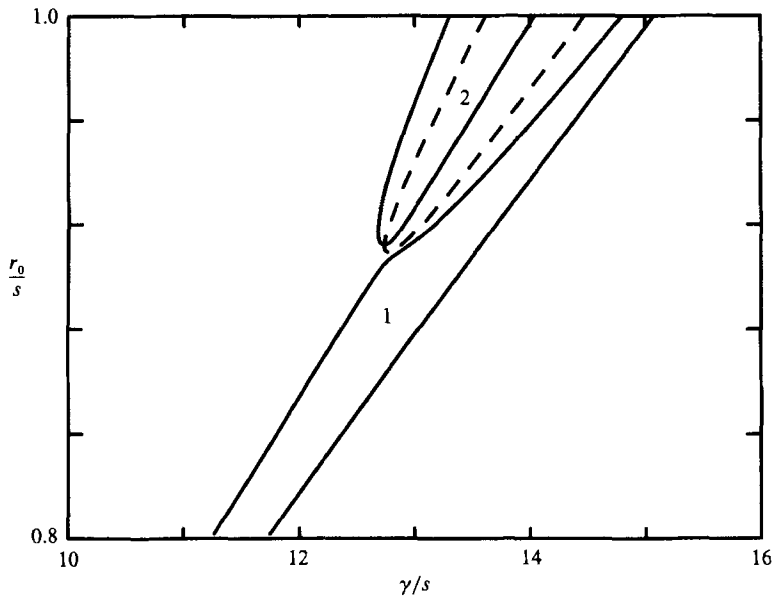
FIGURE 7. Figure 6(c) replotted as r_0 vs γ. The dashed line is the sonic line.

was added to show the behaviour very near the logarithmic singularity in the pressure-time waveform, which occurs at the merging of the two blade areas. The extremum points of each of these retarded airfoil regions (the points of local maximum or minimum r_0 when plotted versus γ) are points at which $\partial f/\partial \gamma = 0$. ($f = \langle c \rangle$ defines the edge of the retarded airfoil shape so that $df = 0$ as one moves along the edge. But $df = (\partial f/\partial \gamma)\,d\gamma + (\partial f/\partial r_0)\,dr_0$ and since $dr_0 = 0$ and $d\gamma \neq 0$ at the extremum, it follows that $\partial f/\partial \gamma = 0$ here.) Thus, the sonic line, $\partial f/\partial \gamma = 0$, passes through each of these extrema. For a straight airfoil it appears that the extrema are always minima, with at most a single extremum on each edge. For a swept blade one can encounter more than one singular point on the leading or trailing edge; i.e. the retarded edge may have a region with both local minima and maxima, as will be seen.

Figure 6(c) is replotted with γ as the abscissa in figure 7, showing more clearly the extremum point that exists at the bottom of the smaller of the two retarded blade regions, here referred to as region 2, with the major blade region being labelled region 1. The sonic line, again shown as a dashed line, passes through the minimum of region 2. When the exact time of the logarithmic singularity in the pressure–time waveform is reached, region 2 in figure 7 meets region 1 at the minimum of the sonic line. (For a swept blade, the two regions generally do not meet at the minimum of the sonic line.) Note that the scale has been magnified to show the details of the region more clearly, and that region 1 comes very close to the sonic line without actually touching; the time is just prior to the occurrence of the logarithmic singularity.

6.2. Singular and nearly singular points

Points satisfying $\partial f/\partial \gamma = 0$ are especially important; in addition to being extrema in a plot of r_0 vs. γ, they are singular points in the integrand of (6) since the denominators of the last two terms in this equation contain the factor $\partial f/\partial \gamma$. Figure 8(a) shows the contribution to the integrand, around the minimum point, r_{sing},
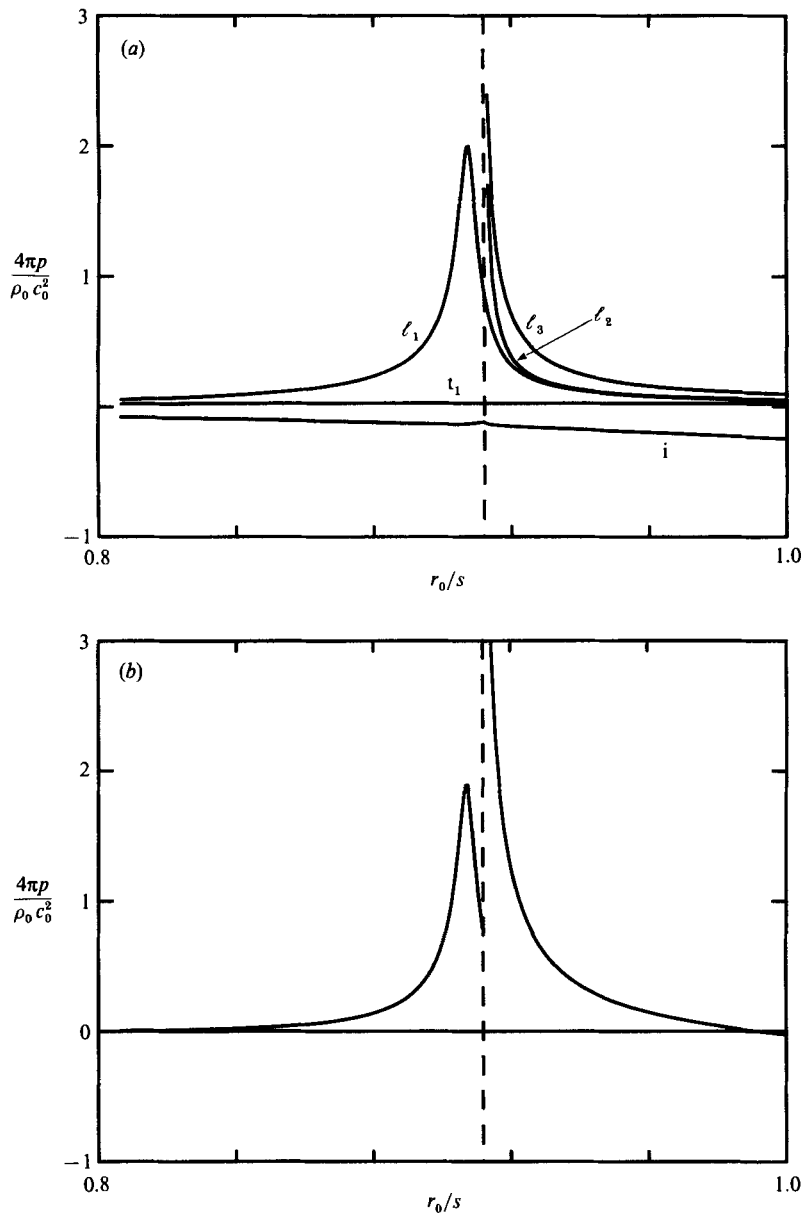
FIGURE 8. Values of the integrand for the r_0-integral in equation (6). The parameters $\Omega r_0/c_0$, $y/s, x, M_x$ take the same values as in figure 5, and $\theta = (\Omega t/2\pi) \times 360 = -177.15$, as for figure 6(c). The dashed line is the radius $r_0/s = 0.912$ of the singular point. ℓ_1 and t_1 are the leading- and trailing-edge contributions from the larger of the two retarded blade areas in figure 6(c). ℓ_2 and ℓ_3 are the edge contributions from the smaller area. i is the γ-integral in equation (6) from both blade areas. (b) Shows the total for all the contributions of (a).

shown in figure 7, for each of the various terms in (6). A 10% thickness biconvex parabolic airfoil, the same as used by Hanson (1976), is assumed with $h(\gamma) = 0.4c\gamma(1-\gamma/c)$. The curve labelled i shows the γ-integral term. The remaining four curves in the figure represent the second and third terms in (6); two of these, ℓ_1 and t_1, represent the leading- and trailing-edge contributions from region 1 and the

remaining two curves, ℓ_2 and ℓ_3, represent the singular contributions from region 2. Beginning at $r_0 > r_{\text{sing}}$, and approaching r_{sing}, the integrand approaches infinity, generally as $\Delta r_0^{-\frac{1}{2}}$ but as Δr_0^{-1} at the time of the logarithmic singularity, where $\Delta r_0 \equiv |r_0 - r_{\text{sing}}|$. There are two contributions of this type since a line drawn at constant r_0 in figure 7 cuts the perimeter of region 2 at two points, both satisfying $f = 0$ representing the leading edge. When r_0 decreases to a value less than r_{sing}, the contribution to the integrand from region 2 immediately drops to zero. This singular behaviour must be properly treated when performing a numerical integration over r_0.

Another difficulty is produced by what will here be called 'near singularities'. This describes very small regions where the integrand becomes large, but not infinite. Whereas a singular point can readily be located by noting where $\partial f / \partial \gamma$ changes sign, the near singularities are not so easily found. A near singularity can arise whenever the retarded source region passes near, but does not intersect, the sonic line given by $\partial f / \partial \gamma = 0$. Such a case is shown in figures 6(c) and 7 where the border of region 1 bulges outward towards the sonic line. On moving along the border of region 1 the factor $\partial f / \partial \gamma$ becomes very small, but never changes sign. The resulting near singularity is shown in figure 8(a); an attempt to locate these regions by searching for rapid changes in the magnitude of the integrand may fail if the step size is too large. A closely related problem occurs if two singularities are more closely spaced than the integration step size. Then a routine looking for a change in sign of $\partial f / \partial \gamma$ can miss both points if a calculation point does not fall between the singular points. Such closely spaced singular points will be seen in the swept-blade cases to follow.

The time corresponding to the case in figure 7 (and for figure 11(c) to be discussed later) was chosen to lie very near to the logarithmic singularity where region 1 approaches very near to the sonic line. As previously noted, at the exact time of the logarithmic singularity, the coefficient of the Δr_0-term in (11) is zero; in this case, retaining additional terms in (11), the relation between $\Delta \gamma$ and Δr_0 near the singularity is

$$\frac{\partial^2 R}{\partial \gamma^2} (\Delta \gamma)^2 + 2 \frac{\partial^2 R}{\partial \gamma \, \partial r_0} \Delta \gamma \, \Delta r_0 + \frac{\partial^2 R}{\partial r_0^2} (\Delta r_0)^2 + \ldots = 0. \tag{23}$$

This is quadratic and has two solutions. Thus, $\Delta \gamma$ and Δr_0 are related in a linear manner, but with two possible slopes emanating from the singular point. This explains the appearance of the corners in the retarded blade shape in figures 6(c) and 11(c). Instead of skirting past the singular point at a reasonable distance, the retarded edge line moves directly towards the singularity then directly away from it. The singularity is never quite reached (unless the time equals precisely the time of occurrence of the logarithmic singularity), but may be approached very closely, forcing the denominator of the second or third terms of (6) very close to zero and producing the near singularity. Thus, these nearly singular points are found near the time and radius of a logarithmic singularity.

Figure 8(b) shows the result from combining the separate terms of figure 8(a). The combined result drops to zero much more quickly than the individual terms as one moves away from the singular point, showing some cancellation between the various terms. Also, it is noted that even if the two singular contributions have been properly computed, a very fine integration scheme is needed to properly account for the very peaked but non-singular contribution.

Performing the r_0-integration gives the pressure at the observer due to all source points. If this is repeated for many time values, a plot of the sound pressure vs. time can be made. Such a plot for the same straight-blade case is shown in figure 9. It
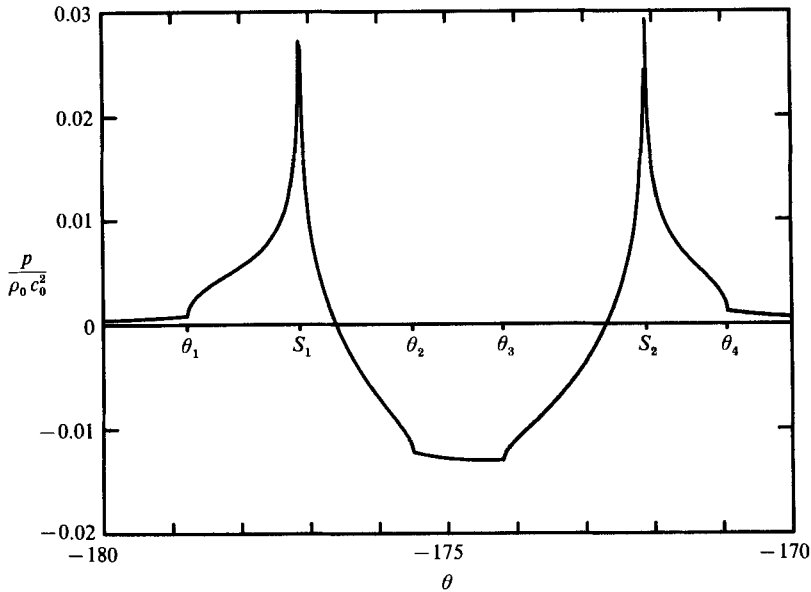
FIGURE 9. Pressure-time waveform for the straight-blade case in figure 6. $\theta_1, \ldots, \theta_4$ and $S_{1,2}$ are given by $\theta_1 = -178.78$, $\theta_2 = -175.50$, $\theta_3 = -174.19$, $\theta_4 = -170.92$, $S_1 = -177.14$, $S_2 = -172.10$.

should be emphasized that no smoothing was done in the creation of this or any of the plots in this paper. All plots were made by a computer-controlled plotter connecting calculated points by straight line segments. This, of course, requires a great many calculated points to get a smooth curve, but it does illustrate the accuracy of the program and gives assurance that there is no prejudicial input on the part of the artist. The abscissa θ represents the angular position of the rotor at the corresponding time. Thus, the abscissa can also be considered a time axis since the angle is linearly related to the time. The angular range θ of the rotor is negative as shown, but would be positive if the next rotor rotation were used for the calculations. The spacing of the calculated points was $0.1°$ or $0.05°$, except near the logarithmic singularities and near the regions of abrupt slope change, for which the spacing was decreased to $0.01°$.

The most prominent feature of this plot is the appearance of two singular points. These are the logarithmic singularities; they appear where the factor multiplying Δr_0 in (11) (repeated in (14)) becomes zero. Because linear theory gives a singularity at these points, one cannot calculate a magnitude for the peak. The value calculated for the trough, however, can be compared with the previous calculation of Hanson (1976) for this case. Hanson gives $p/\rho_0 c_0^2 = -0.013$, while the present calculation gives -0.012970 for the minimum value attained. The present result thus agrees with that of Hanson, but Hanson's result does not resolve the fine detail shown in figure 9; the relatively flat botom of the curve is not at all evident. A similar, but not identical case, calculated in the frequency domain, is given in figure 5 of Hawkings & Lowson (1974), but this also fails to show the fine detail.

6.3. *Points of abrupt change of slope*

In addition to the logarithmic singularities in the plot of pressure versus time, there are points, θ_1, θ_2, θ_3, θ_4, where the plot abruptly changes slope. These points correspond to the appearance or disappearance of the second retarded blade source

region. As noted from figures 6 and 11, this new region originates at the blade tip and grows inward. (The sequence of events is slightly different for the 50° sweep case.) Since there is always a singular point at the minimum r_0-value of region 2 shown in figure 7, when region 2 first arises it does so with the appearance of a singularity at the tip. This occurs when the leading edge becomes sonic at the tip with respect to the fluid-fixed observer; the appearance of the source region is shown at the upper end of the sonic line near the 30° angle of the rotor disk at a time between the values of figure 6(a) and (b). The region then expands as the singularity moves inward along the edge. θ_2 corresponds to the disappearance of the singular point from the rotor leading-edge tip around the angle of $-25°$, as shown in figure 6(e) in which one can just see region 2 at the lower end of the dashed sonic line. θ_3 and θ_4 relate to the trailing edge, around the times corresponding to figures 6(g), which shows the appearance of a singular point, and 6(j) which shows its disappearance. These θ_n-values can readily be calculated in the following manner: (i) calculate the two γ-values of the sonic line at the tip; (ii) introduce these into (4) to find the corresponding R values; (iii) introduce these γ- and R-values into (8) from which four values of time t can be determined; θ then follows from $\theta = \Omega t$.

The slope of the pressure-time waveform is infinite at these θ-values. Since the velocity v_s of the singular point along the edge is generally non-zero when the singularity enters the tip, the distance d of the singularity from the tip is $d = v_s \Delta t$ for small $\Delta t \equiv t - t_0$, where t_0 is the time of appearance of a singularity at the tip. Performing the r_0-integral in (6) over the $r_0^{-\frac{1}{2}}$ singularity gives, for the contribution of the newly formed region,

$$I \sim \int_0^d \frac{dr_0}{r_0^{\frac{1}{2}}} = 2d^{\frac{1}{2}} = (v_s \Delta t)^{\frac{1}{2}}. \tag{24}$$

The time derivative, or slope, thus varies as $(\Delta t)^{-\frac{1}{2}}$ near each $\theta_1, \ldots, \theta_4$ value; this is infinite for $\Delta t = 0$.

The relative importance that the various portions of the pressure–time waveform have in generating the overall acoustic intensity at the observer is found by squaring the pressure and integrating with respect to time with a variable upper limit. Figure 10, with the upper limit as abscissa, shows that singular regions are important, but do not dominate over the remainder of the waveform. The large negative portion of the waveform is somewhat more important for this particular case.

6.4. Effect of sweep

The result of sweeping the blade a moderate amount, but not enough to eliminate the logarithmic singularities is shown in figures 11 and 12. The rotor blade is identical to the straight blade, except for the tip region, which is swept back at approximately a 20° angle, keeping constant the chord measured along γ. The planforms for the three cases of straight blade, 20° and 50° sweep are shown in figure 13(h–j); these plots are created from the same program and blade inputs used for calculating the retarded blade shapes and pressure, but now assuming zero Mach number. Defining r_1 as the value of r_0 at the break point A in figure 3 where the airfoil begins to sweep, the blade definition for $r_0 > r_1$ is

$$\gamma_0 = \chi(r_0 - r_1) = r_0 \epsilon, \tag{25a}$$

where $\chi = \tan(20°)$ for figures 11 and 12 and γ_0 is the arc DE. This definition was simpler than a constant angle of sweep since the definition was made in the (r_0, γ)-coordinate system, but as noted from figure 13(i) and (j), the deviation from a constant sweep angle is small. The value of ϵ is not needed in the calculations, but
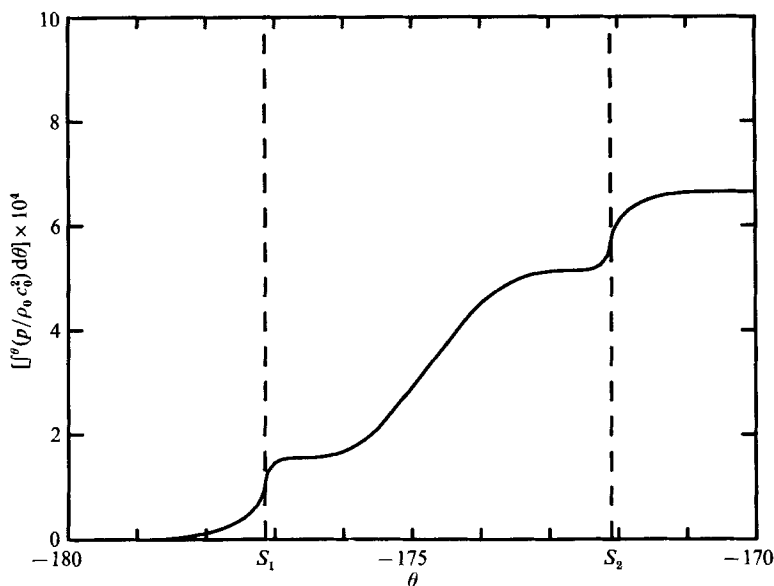
FIGURE 10. Time integral of the acoustic intensity at the observer as a function of time (angle).

can be used in the following equation to find the local slope δ of the blade. From the geometry of figure 3,

$$\tan(\delta - \epsilon) + \epsilon = \chi. \tag{25b}$$

For values of ϵ not too large, $\tan \delta$ is nearly constant and close to the value assumed for χ.

The retarded blade shapes in figure 11 are topologically quite similar to those in figure 6. The time between plots is now not fixed at $1°$ increments to allow selection of the most interesting cases. Figure 11 (c) shows the retarded blade shape at a time very near to but just before the appearance of the logarithmic singularity. The two separate blade regions have not quite merged yet; enlarging the region near the merger point would show the two retarded blade areas to be in the shape of two corners that have not quite met. The points $\theta_1, \ldots, \theta_4$ are determined by the time at which the tip of the leading or trailing edge intersects the sonic line; since the sonic line is the same for both cases, as is the airfoil chord measured along the γ-coordinate, the spacing between these points is the same in figure 12 as in figure 9. The logarithmic singularities, S_1 and S_2, have shifted left relative to $\theta_1, \ldots, \theta_4$ when compared to figure 9. The minimum in the curve is now $p/\rho c_0^2 = -0.01135$, not radically different from the value for the straight-blade case. One notes that the relatively flat portion of the curve between θ_2 and θ_3 in figure 9 has now begun to tilt upward to the right.

One additional point worth noting is that several singular points in the r_0-integral can now exist on the leading or trailing edge. Thus, three singular points in the r_0-integral are evident on the leading edge of figure 11 (b). The two singular points produced at the two corners noted above lie very close to one another, and provision must be made in the computer program for resolution of the points. Two closely spaced points are also found for a very short time slightly prior to that shown in figure 11 (b) when the rotor retarded planform just crosses the sonic line.

Figures 13 and 14 show similar calculations for the $50°$ sweep case ($\chi = \tan(50°)$). This calculation is more subject to error than the $20°$ case, because of the significant
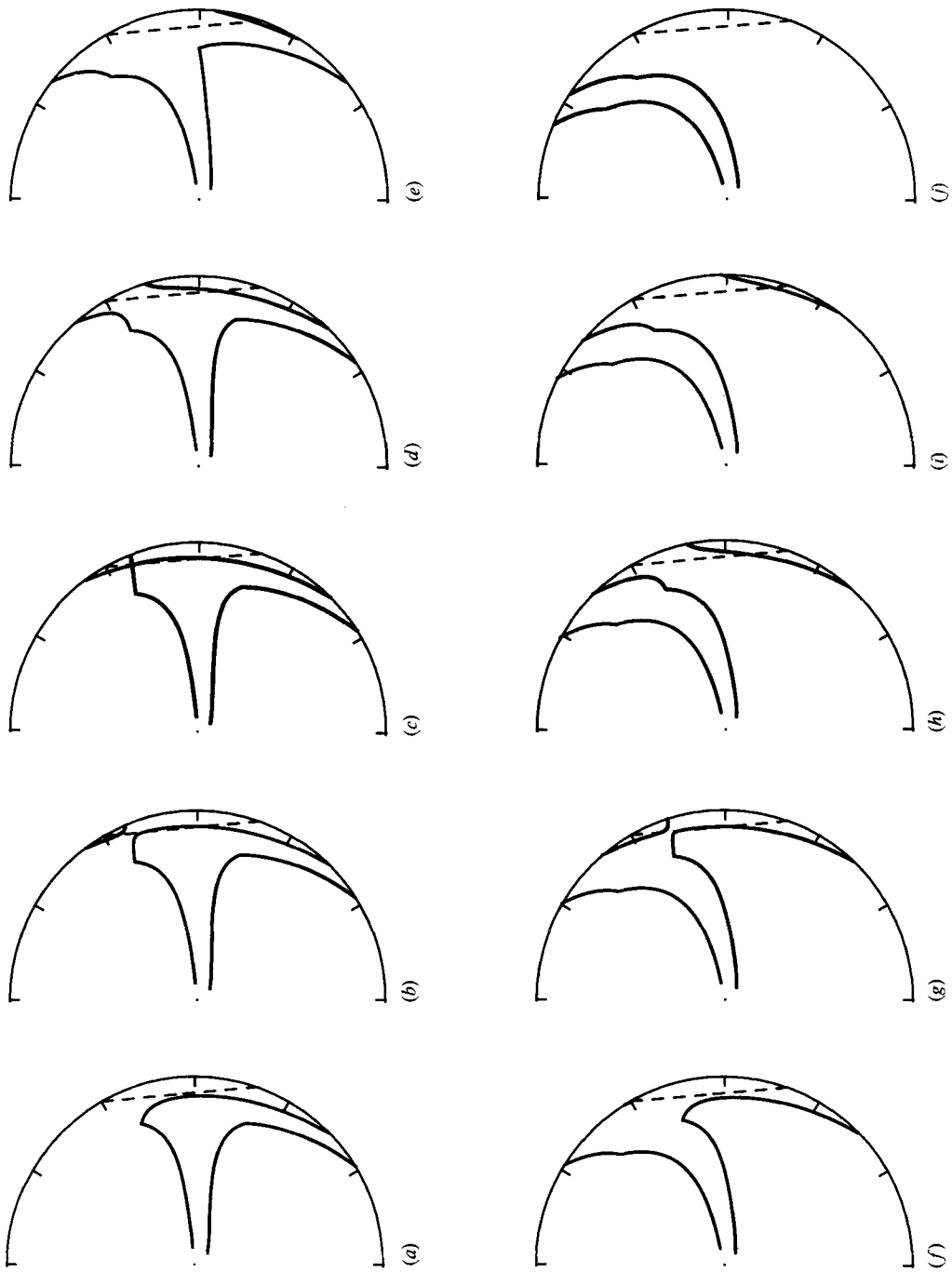
FIGURE 11. Retarded blade shapes under the same conditions as figure 6, but for a 20° sweep at the outer 20% of the blade; the blade shape is shown in figure 13(*i*). (*a*) $\theta = -175$; (*b*) -174.4; (*c*) -174.353; (*d*) -174; (*e*) -172; (*f*) -170; (*g*) -169.5; (*h*) -169; (*i*) -168; (*j*) -166.
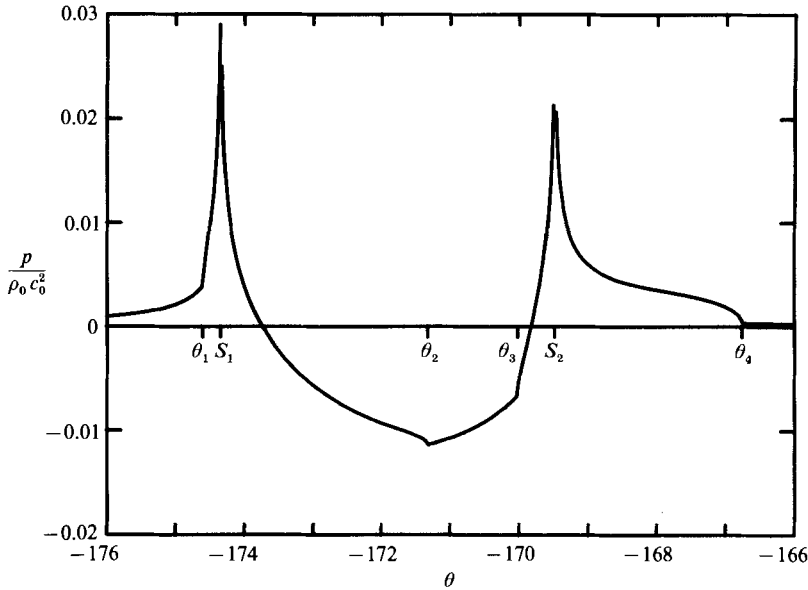
FIGURE 12. Pressure–time waveform corresponding to figure 11. $\theta_1, \ldots, \theta_4$ and $S_{1,2}$ are given by $\theta_1 = -174.61$, $\theta_2 = -171.33$, $\theta_3 = -170.02$, $\theta_4 = -166.75$, $S_1 = -174.35$, $S_2 = -169.48$.

cancellation produced by the sweep in the radial integration. The logarithmic singularities, S_1 and S_2, are no longer present; their absence means that blade areas cannot split off or merge inboard of the tip. Thus, as time proceeds from figure 13(e) to (g), the r_0-singularity moves upward towards the observer along the sonic line. The second blade area does not split off as in figures 6(i) and 11(h) (which would produce a logarithmic singularity); rather, the r_0 singularity first reaches the rotor tip, defining the θ_3 point and beginning a rapid decrease in the far-field pressure. A dramatic reduction in the sound results when compared to the straight-blade and 20° sweep cases.

The spacing of the points $\theta_1, \ldots, \theta_4$ is the same as for the straight-blade and the 20° sweep cases. The effects produced by the points $\theta_1, \ldots, \theta_4$ has changed, however. Thus, for the straight-blade case θ_1 is the angle at which the second area along with a singular point (representing a minimum in the r_0 *vs.* γ curve as in figure 7) are created just prior to figure 6(b), beginning an increase in the pressure waveform. For the 50° sweep case, θ_1 is the angle at which a singular point (representing a maximum in the r_0 *vs.* γ curve) leaves the blade just prior to figure 13(c), beginning a decrease in the pressure. Whereas the singularity for the straight-blade case gives a contribution to the integral for $r_0 > r_{\text{sing}}$ (where r_{sing} denotes the radius at the singular point), the singular point for the 50° sweep case gives a contribution to the integral for $r_0 < r_{\text{sing}}$. θ_2 and θ_4 are produced by similar circumstances for the straight and 50° sweep cases, but θ_3 marks a singular point entering the straight blade, just prior to figure 6(g), beginning an increase in the pressure waveform, while θ_3 marks the disappearance of a singular point from the 50° swept blade, just after figure 13(e), beginning a decrease in the pressure waveform.

One might look to the possibility of varying the timing of the θ_n-values as a means to control the sound. For any given span and angular velocity the spacing between the pair θ_1, θ_2 is fixed for any given observer position, as is that between the pair θ_3, θ_4. The first of these pairs is produced by the leading edge at the tip crossing first one end then the other end of the sonic line; the second pair is produced in a similar
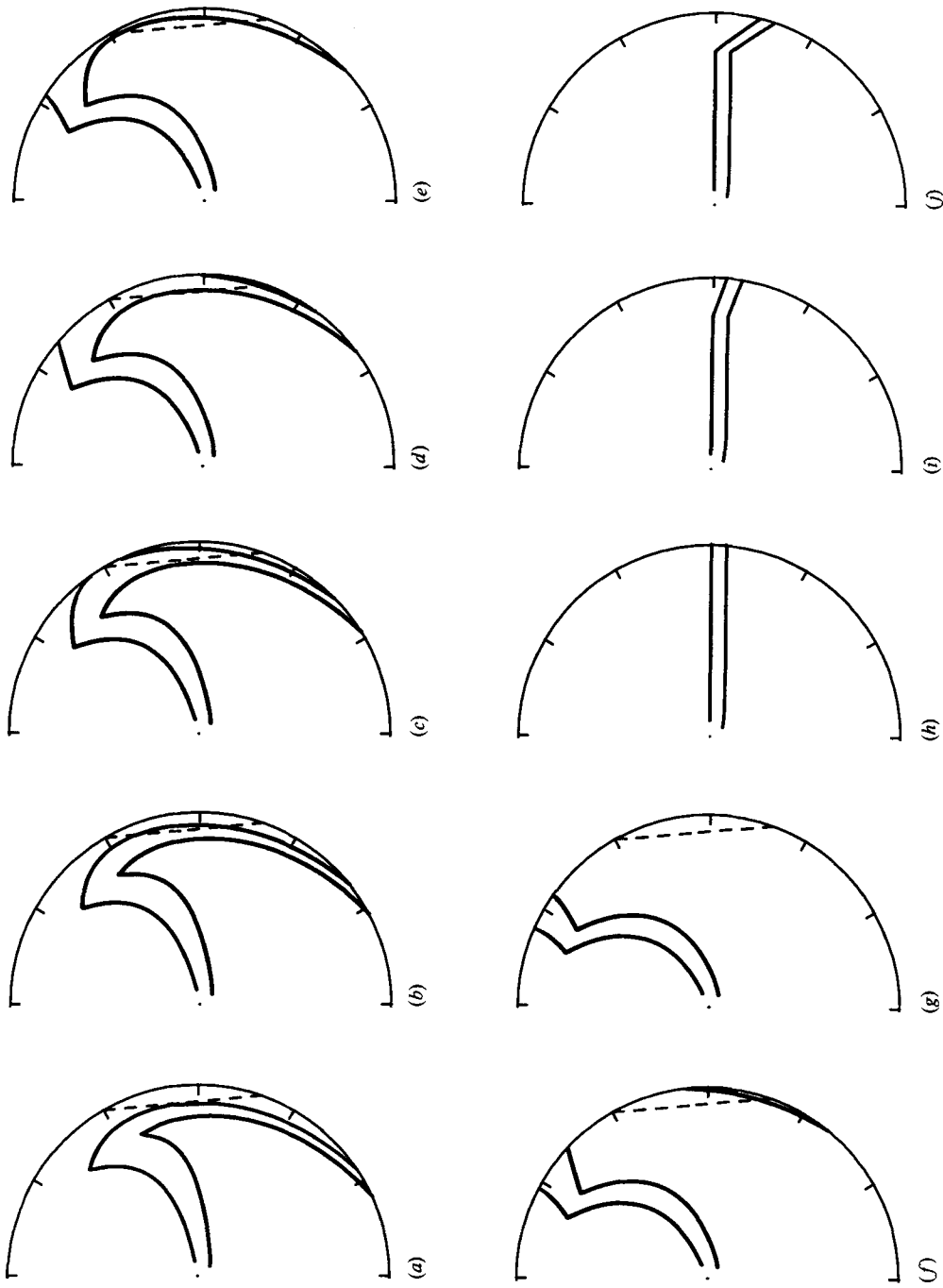
FIGURE 13. Retarded blade shapes under the same conditions as figure 6, but for a 50° sweep at the outer 20 % of the blade. (h–j) show the blade shapes for the three cases of straight blade, 20° sweep and 50° sweep. (a) $\theta = -169$; (b) -167; (c) -165; (d) -163; (e) -161; (f) -159; (g) -157.
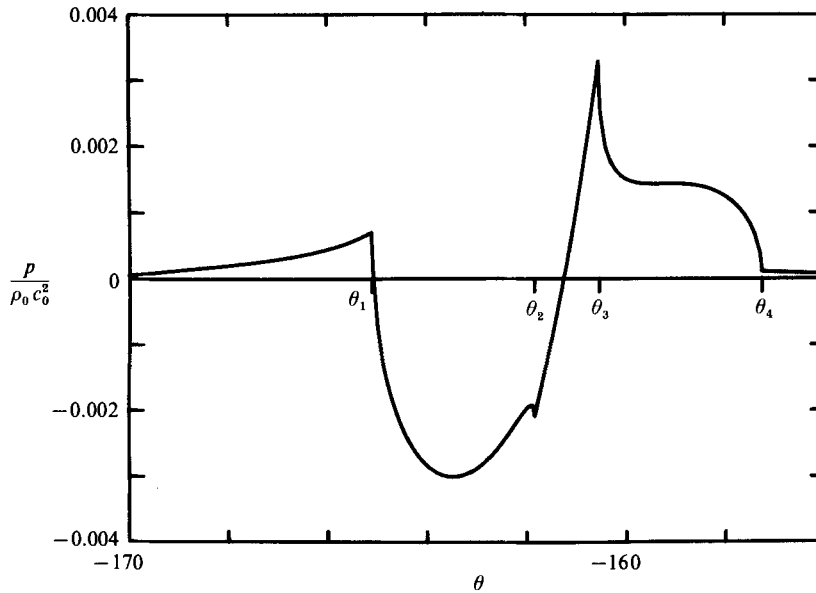
FIGURE 14. Pressure–time waveform corresponding to figure 13. $\theta_1, \ldots, \theta_4$ are given by
$\theta_1 = -165.12$, $\theta_2 = -161.85$, $\theta_3 = -160.54$, $\theta_4 = -157.26$.

manner by the trailing edge. Changing the chord does not change the spacing between these pairs. However, the spacing between θ_1 and θ_3 (or between θ_2 and θ_4) is dependent on the value of the chord at the rotor tip, since the θ_1, θ_3 spacing is determined by the time between when the leading edge crosses one end of the sonic line and when the trailing edge crosses the same point. The time t_0 between θ_1 and θ_3 is $t_0 = c/U$; thus, for the present $V = 0$ case the angular spacing between these points is $\Omega t_0 = c/s = 4.58°$ for $c/s = 0.08$, agreeing with figures 9, 12 and 14. The capability of varying the spacing between θ_1 and θ_3 by varying the chord at the tip might be worth further investigation as a means of noise control. The θ_n values do not give the complete explanation of the waveform, however. Thus, in figure 14 there is a sharp increase in the pressure waveform between θ_2 and θ_3, even though there are no singular points entering or leaving the tip of the blade.

7. Conclusion

Success in the reduction of the thickness noise produced by a propeller is dependent on understanding the mechanism of sound production. The preceding analysis and comparison with numerical calculations gives a better description of the sound generation process than previously available. The numerical techniques used completely eliminate the sometimes erratic behaviour of previous calculations and show that the result for linearized flow should be a perfectly smooth pressure–time waveform, except at the logarithmic singular points, and at four other points at which the slope changes abruptly for an airfoil with a sharp leading edge. These abrupt slope changes are produced by a singular point entering or leaving the rotor at the tip. The results show the feasibility of performing calculations in the time domain, which has sometimes been bypassed in favour of frequency-domain calculations in order to avoid certain computational difficulties, even though the time-domain calculation may be more instructive. Although the initial programming task is difficult for the time-domain calculation, it need only be performed once.

Examples have been given for three straight- and swept-blade cases, consisting of

nearly straight line segments for the leading and trailing edges. It should be emphasized that the general case of a blade with a smoothly increasing sweep near the tip is a more realistic one and may produce a waveform that looks somewhat different. It should be possible to significantly influence the waveform by changing the sweep, chord and thickness distribution. Nevertheless, all waveforms will exhibit the four points $\theta_1, \ldots, \theta_4$ as distinct features since they are produced whenever either the leading or trailing edge crosses the sonic line. An exception to this would appear to be the case where the chord has tapered to zero at the tip; the leading and trailing edge θ-values are then superimposed, θ_1 on θ_3, and θ_2 on θ_4.

Logarithmic singularities may also be present, although a proper blade design should eliminate them. They may be prevented for a given observer by avoiding areas on the blade that can move sonically relative to an observer while simultaneously having the edge normal to the source–observer line. To eliminate the logarithmic singularities throughout the flow field requires that the component of the rotor-blade Mach number normal to the edge be everywhere subsonic. Hopefully, understanding these logarithmic singularities together with an understanding of the role played by the four θ_n-values, as well as the ability to adjust the spacing between them to some extent, will prove useful in noise reduction.

This paper is dedicated to Professor William R. Sears on the occasion of his 75th birthday.

REFERENCES

AMIET, R. K. 1977 Thickness noise of a propeller or helicopter rotor. *United Technologies Research Center Rep.* R77–111204.

CURL, N. 1955 The influence of solid boundaries upon aerodynamic sound. *Proc. Roy. Soc. Lond.* A231, 505–514.

FARASSAT, F. 1983 The prediction of the noise of supersonic propellers in the time domain – new theoretical results. *AIAA Paper* 83-0743.

FARASSAT, F. 1984 The unified acoustic and aerodynamic prediction theory of advanced propellers in the time domain. *AIAA Paper* 84-2303, *AIAA/NASA 9th Aeroacoustics Conference, October 15–17, 1984, Williamsburg, Virginia, USA*.

FARASSAT, F. 1986 Prediction of advanced propeller noise in the time domain. *AIAA J.* 24, 578–584.

FARASSAT, F. & SUCCI, G. P. 1980 A review of propeller discrete noise prediction technology with emphasis on two current methods for time domain calculations. *J. Sound Vib.* 71, 399–419.

HANSON, D. B. 1976 Near field noise of high tip speed propellers in forward flight. *AIAA Paper* 76-505, *AIAA 3rd Aeroacoustics Conference, July 20–23, 1976, Palo Alto, California, USA*.

HANSON, D. B. 1979 The aeroacoustics of advanced turbopropellers. In *Mechanics of Sound Generation in Flows* (ed. E.-A. Muller), IUTAM/ICA/AIAA-Symposium, Gottingen, pp. 282–293.

HANSON, D. B. 1980 The influence of propeller design parameters on far field harmonic noise in forward flight. *AIAA J.* 18, 1313–1319.

HAWKINGS, D. L. & LOWSON, M. V. 1974 Theory of open supersonic rotor noise. *J. Sound Vib.* 36, 1–20.

HILTON, W. F. 1938 The photography of airscrew sound waves. *Proc. R. Soc. Lond.* A169, 174–190.

LOWSON, M. V. & JUPE, R. J. 1974 Wave forms for a supersonic rotor. *J. Sound Vib.* 37, 475–489.

SCHMITZ, F. H. & YU, H. 1986 Helicopter impulsive noise: theoretical and experimental status. *J. Sound Vib.* 109, 361–422.

TAM, C. K. W. 1983 On linear acoustic solutions of high speed helicopter impulsive noise problems. *J. Sound Vib.* 89, 119–134.